



This is a repository copy of *Experimental investigation of the influence of solidity on the performance and flow field aerodynamics of vertical axis wind turbines at low Reynolds numbers*.

White Rose Research Online URL for this paper:
<http://eprints.whiterose.ac.uk/95454/>

Version: Accepted Version

Article:

Eboibi, O., Danao, L.A.M. and Howell, R.J. (2016) Experimental investigation of the influence of solidity on the performance and flow field aerodynamics of vertical axis wind turbines at low Reynolds numbers. *Renewable Energy*, 92. pp. 474-483. ISSN 0960-1481

<https://doi.org/10.1016/j.renene.2016.02.028>

Article available under the terms of the CC-BY-NC-ND licence
(<https://creativecommons.org/licenses/by-nc-nd/4.0/>)

Reuse

Unless indicated otherwise, fulltext items are protected by copyright with all rights reserved. The copyright exception in section 29 of the Copyright, Designs and Patents Act 1988 allows the making of a single copy solely for the purpose of non-commercial research or private study within the limits of fair dealing. The publisher or other rights-holder may allow further reproduction and re-use of this version - refer to the White Rose Research Online record for this item. Where records identify the publisher as the copyright holder, users can verify any specific terms of use on the publisher's website.

Takedown

If you consider content in White Rose Research Online to be in breach of UK law, please notify us by emailing eprints@whiterose.ac.uk including the URL of the record and the reason for the withdrawal request.



eprints@whiterose.ac.uk
<https://eprints.whiterose.ac.uk/>

Experimental Investigation of the Influence of Solidity on the Performance and Flow Field Aerodynamics of Vertical Axis Wind Turbines at Low Reynolds Numbers

Okeoghene Eboibi¹, (+2348069477913, o.eboibi@gmail.com), Louis Angelo M. Danao², Robert J. Howell³

Abstract

This paper shows the results of an experimental investigation into the effect of changes in solidity on the performance of a Vertical Axis Wind Turbine. Two VAWT configurations are used, one of solidity $\sigma = 0.26$ (chord $C = 0.03\text{m}$) and the other with $\sigma = 0.34$ ($C = 0.04\text{m}$). The turbine performance coefficient (C_p) was measured over a range of tip speed ratios and Particle Image Velocimetry (PIV) was used to determine the flow field around both turbine configurations.

Performance (C_p - λ) curves for the two VAWTs are compared at the same Reynolds numbers to investigate the effects of solidity alone on the performance and aerodynamics of each configuration. The higher solidity ($\sigma = 0.34$) VAWT attained a similar maximum C_p but with a narrower C_p - λ curve than the lower solidity VAWT. The performance differences between the two VAWT configurations at two tip speed ratios are explained in detail using PIV around both VAWT rotor blades. This allows the linking of detailed aerodynamics to the performance and it was shown that the generation and shedding of stall vortices started earlier on the lower solidity VAWT than the higher solidity VAWT, thus limiting the rotor efficiency.

Keywords: Solidity; Performance; PIV; VAWT; HAWT

Nomenclature

A	rotor frontal swept area, 2RL	ρ_f	fluid density
AR	aspect ratio	V_w	free stream wind speed
C	blade chord	v_s	settling velocity
C_p	power coefficient	R_p	particle radius
Re	Reynolds number	μ_f	fluid viscosity
G	acceleration due to gravity	λ	tip speed ratio, $R\omega/V_\infty$
I_{rig}	rotor rotational mass moment of inertia	ξ	rotor angular acceleration
L	blade length	ρ	air density
N	number of blades	σ	rotor solidity, Nc/r
P_B	blade power	ω	rotor angular speed
P_w	wind power	CFD	Computational fluid dynamics
R	rotor radius	HAWT	Horizontal axis wind turbine
T_{app}	applied brake torque	LEV	Leading edge vortex
T_B	blade torque	TEV	Trailing edge vortex
T_{res}	resistive torque	VAWT	Vertical axis wind turbine

¹ Senior Lecturer, Department of Mechanical Engineering, Delta State Polytechnic, Ozoro, Nigeria.

² Associate Professor, Department of Mechanical Engineering, University of the Philippines, Quezon City, Philippines.

³ Senior Lecturer, Department of Mechanical Engineering, University of Sheffield, Sheffield, U.K.

1.0 Introduction

The demand for energy continually increases but the supply of affordable and reliable electricity to meet the needs of the growing population is lacking in many developing nations such as Nigeria. For example, Nigeria has a population of over 170 million but generates a meagre peak of 6GW of electricity, whereas Brazil with a population of about 190 million generates over 200GW of electricity, Abdul-Malik et al. (2009). To meet the growing demand while protecting the environment from the effects of greenhouse gas emissions, electricity is being generated from renewable sources such as sun, through the use of solar cells, and wind, through the use of wind turbines.

The horizontal axis wind turbines (HAWT) are well established for the commercial generation of electricity, partly due to many years of research and development that they have enjoyed. Vertical axis wind turbines (VAWT) are currently the subject of research due to some advantages they appear to have over the HAWT. For example, the Darrieus VAWT is a simple design with two or three fixed symmetrical blades, operates at lower tip speed ratios, and does not requiring any yaw control, while the geometry of the HAWT rotor blade is more complex with blades that twist and taper and often require a yaw mechanism (Klimas, 1982). Lower tip speed ratios mean that there is a potential for the VAWT to have lower noise than a HAWT. However, the advantage enjoyed by the VAWT's simple geometry is limited by the complex aerodynamics and lack of self-starting ability. VAWT aerodynamics are non-linear and highly unsteady, (Beri and Yao, 2011), due to the large changes in angle of the attack as the VAWT blades rotates which results in complex structural dynamics caused by fluid structure interactions.

1.1 Related Literature

Templin (1974) and Sheldahl et al, (1974) defined VAWT solidity as expressed in Equation (1) and this solidity can be changed by altering the number of blades, the blade chord or the rotor radius. Templin (1974) used single stream tube momentum model to study the effects of solidity within a range of $\sigma = 0.05$ to 0.5 , on the performance of VAWT by changing the number of blades.

$$\sigma = \frac{Nc}{r} \quad (1)$$

Mays and Holmes (1979) also used a momentum model to study the effects of high solidity, $\sigma = 0.75$, on the performance of vertical axis windmill. The results of May and Holmes (1979) investigation complemented the works of Templin (1974). The trends of the performance curves of the two studies were similar when compared by Kirke (1980). Consul et al. (2009) used commercial Computational Fluid Dynamics (CFD) software to investigate the influence of solidity on the hydrodynamics of a tidal cross-flow turbine by simulating flows through 2D two- and four- bladed turbines with corresponding solidities of 0.019 and 0.038 . Consul et al. (2009) observed peak power

coefficient of 0.43 and 0.53 for the two- and four-bladed turbine respectively with a shift of the four-bladed turbine's power curve to lower tip speed ratios.

Recently, Howell et al. (2010) experimentally compared the performance of small wind tunnel scaled two- and three-bladed VAWTs and affirmed that the two bladed VAWT attained a higher C_p at a higher tip speed ratio, while the three-bladed VAWT attained lower C_p at lower tip speed ratio. The results of Howell et al (2010) investigation contradict the revelation of the earlier studies probably due to differences in the investigative methods employed. Although, a two bladed VAWT was not tested, Raciti Castelli et al. (2012) in their study, in which three-, four- and five-bladed VAWT of NACA0015 profile were compared using CFD, it was shown that the three-bladed VAWT performed better than the other configurations tested. Considering the investigations of Raciti Castelli et al. (2012) and Howell et al. (2010), there is no economic justification to increase the number of VAWT blades beyond three. A summary of the previous research is presented in Table 1 and all investigations showed that turbine solidity has a large effect on the performance of a turbine.

Author	Configuration Tested	VAWT scale	Method of investigation	Compared data
Templin (1974)	One – six bladed VAWT of NACA0012 profile	Above 5Kw	Momentum Model	Power coefficient
Mays and Holmes (1979)	N/A	Above 5Kw	Momentum Model	Power coefficient
Consul et al. (2009)	Two and four bladed VAWT of NACA0015	5 Kw scale	Computational Fluid Dynamics	Power coefficient efficiency and velocity vectors
Howell et al. (2010)	Two and three bladed VAWT of NACA0022 profile	Small wind tunnel scale	Experimental	Power coefficient
Raciti Castelli et al. (2012)	Three, four and five bladed VAWT of NACA0025 profile	Small wind turbine	Computational Fluid Dynamics	Power coefficient and absolute velocity contours

Table 1 Summary of most important literature reviewed

All previous studies, in which attempts have been made to investigate solidity, have been carried out by varying the number of blades (Table 1). This paper seeks to experimentally investigate the influence of solidity on performance and flow field aerodynamics of VAWT by altering the blade chord as well as to understand the aerodynamic causes of the changes in turbine performance. The aim shall be achieved through the following primary objectives:

- i. Experimental measurements to determine the power coefficients of the two VAWT configurations at three wind speeds and at a range of tip speed ratios (λ).
- ii. PIV visualisation measurements of the flow fields around the blades of the turbines at $\lambda = 2.5$ and 3, and at the same Reynolds number.

2.0 Methods

The experiments were conducted in the University of Sheffield low speed, open-circuit suction wind tunnel (Figure 1). The working section is 1.2 x 1.2m and 3m long with a turbulence intensity of around 1% at the turbine location. The VAWT geometry has a central shaft diameter of 0.027m that runs across the wind tunnel test section from top to bottom. The rotor central shaft is positioned 1.8m from the upwind and 1.2m downwind of the wind tunnel test section. There are two hubs rigidly attached to the shaft, with provisions for the attachment of the support arms that connect the blades to the centre shaft at $\frac{1}{4}$ and $\frac{3}{4}$ rotor blade length. The turbine radius is 0.35m. The blades are made of aluminium with a NACA0022 profile and 600mm span, while the support arms are NACA0026. The two sets of blades were made with chords of $C = 0.03\text{m}$ (termed Blade 1) and with $C = 0.04\text{m}$ (termed Blade 2) with resulting solidities of 0.26 and 0.34 respectively.

Measurements for rotor performance data were logged (Table 2) using a National Instruments data acquisitions card (model PCI-6220). To measure rotational velocity, an Avago optical encoder (model AEDA-3300-TAM) was used with a resolution of 3000 pulses per revolution. A second channel with a 1 pulse per revolution was also available for syncing blade position with the flow visualization apparatus (discussed later in this section). Wind velocity measurements were carried out using a Dantec constant temperature hotwire anemometer (model Type 55 P16), calibrated daily with reference to a Furness Controls micro-manometer (model FCO510).

Test/Activity	Equipment Used
Data logging	National Instruments (model: PCI-6220) data acquisitions card
Rotational velocity	Avago optical encoder (model: AEDA-3300-TAM) with 3000 pulses per revolution and 1 pulse per revolution
Wind velocity	constant temperature hotwire anemometer (probe model: Dantec Type 55 P16)
Applied brake	Magtrol hysteresis brake (model: HB-140-M2)
Applied torque	Sangamo DC miniature displacement transducer (model: DFG/2.5)

Table 2. Instrumentation used in the turbulence measurement experiments.

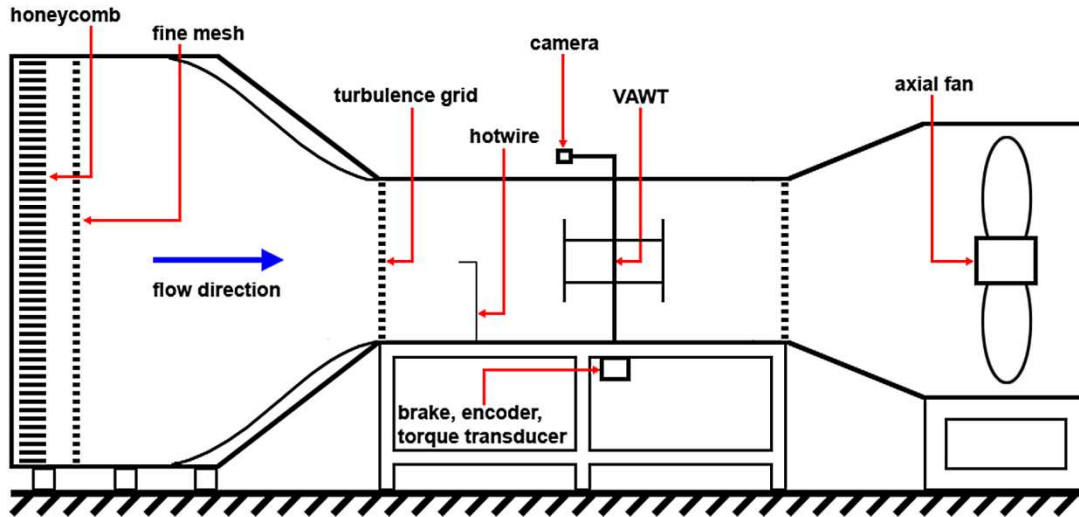


Figure 1. Schematic of the wind tunnel and experimental set up.

Torque was not measured directly but derived from a fundamental relationship between the moment of inertia of the turbine systems and its acceleration (see Section 2.1) developed in Sheffield. For tests requiring an applied brake to prevent rotor over speed, a Magtrol hysteresis brake (model HB-140-M2) was available. The brake is mounted on a spring balance and a Sangamo DC miniature displacement transducer (model DFG/2.5) measures the linear displacement of the transducer core attached to a point on the balance with known lever arm length. The transducer voltage was calibrated by loading the system with static standard weights. The error in velocity measurement (the largest source of error) results in a performance coefficient error of around $\pm 1\%$ at $\lambda = 4$ and 7m/s wind speed.

A Dantec Dynamics 2D PIV system was used for all the PIV visualization tests in this study. The system has a Litron Nano-S-65 Nd:YAG laser that emitted light at a maximum energy of 65mJ per pulse and wavelength of 520nm. A 4 megapixel (CCD) camera was used to capture the images. A TSI 9306A Six Jet Atomiser generated the tracer particles from olive oil that had an approximate size of $2\mu\text{m}$ in diameter. To synchronize the image acquisition with the moving blade, the camera was triggered using the signal from the optical encoder's 1 pulse per revolution channel. The trigger point was manually set together with the camera position.

2.1 Power coefficient measurements

The performance of the turbines was measured using the so-called 'spin down' method developed in Sheffield by Edwards et al. (2012). The method involves the spinning down of the rotor from a high rotational speed, while the angular velocity is monitored through the optical encoder and the instantaneous deceleration ξ computed by Equation (2).

$$\xi = \frac{\omega_2 - \omega_1}{t_2 - t_1} \quad (2)$$

For each test wind speed, the rotor is spun twice to determine the performance of the VAWT. The first spinning down of the rotor is aimed at determining the resistive torque of the rig. The resistive torque T_{res} is determined by spinning the rotor down without the blades attached to measure the system resistance caused by the mechanical friction, bearings and the support drag of the support arms. Since the blades are not attached to the rotor during the resistive torque tests, the application of brake is not necessary irrespective of the wind speed the test was conducted, because no positive torque is generated. The T_{res} is computed after the test by using Equation (3).

$$T_{res} = I_{rig} \xi \quad (3)$$

The second spin down test is carried out with the blades attached and allows the determination of the performance of the VAWT based on the blade torque. An additional (and known) braking force was necessary to force the turbine to decelerate (spin down) at wind speeds of 7m/s and 8m/s. The aerodynamic torque generated by the blades, T_B , is computed using Equation (4), where the applied torque, $T_{app} = 0$ for cases in which brake power was not applied. Other details of the development and verification of the spin down method are found in Danao (2012).

$$T_B = I_{rig} \xi - T_{res} - T_{app} \quad (4)$$

$$C_p = \frac{P_B}{P_w}, \quad P_B = T_B \omega N, \quad P_w = 0.5 \rho A V_w^3 \quad (5)$$

The power coefficient of the VAWT based on the blade torque was computed using Equation (5) after determining the T_B from the spin-down tests. The determined VAWT power coefficient C_p of the two configurations at the three wind speeds is presented and discussed in section 3.1.

2.2. Flow field visualization measurements

Fujisawa and Shibuya (2001), and Simao-Ferreira et al. (2009) were the earliest investigators that used PIV in the investigation of the flow environment around VAWT blades. Fujisawa and Shibuya (2001) conducted PIV tests on a single bladed VAWT at a very low Reynolds number of 3000 and they also injected dye in the water tunnel to aid flow visualisation. Fujisawa and Shibuya, (2001) revealed two pairs of shed stall vortices that occur in a rotor blade cycle and also that there was a dependence of shed stall vortices (size and dynamics) on turbine tip speed ratio. Simao-Ferreira et al. (2009) conducted their tests on a one-bladed rotor in a wind tunnel, at $Re = 50,000$ and $70,000$ and validated a 2D CFD model with that data. Those Reynolds numbers are similar to those used in this investigation. More recently, while improving on the previous PIV studies of VAWTs through measurement of the flow around a blade at more azimuth positions and also revealing the effects of

flow reattachment to a blade surface, Edwards et al. (2013) and Eboibi et al.(2014) have investigated the flow environment around a blade of a three bladed VAWT.

The accuracy with which the tracer particles follow fluid stream was determined by estimating the settling velocity of the particles in relation to the fluid motion through Equation (6). The particle settling velocity was estimated to be 0.0001m/s which is negligible when compared to the 6m/s wind speeds at which the PIV tests were conducted, signifying that the particles would follow the fluid motion faithfully without significantly deviating from the fluid streamlines even during periods of rapid changes in flow direction as a result of flow separation.

$$v_s = \frac{2gR_p^2(\rho_p - \rho_f)}{9\mu_f} \quad (6)$$

The rotor blade surfaces were treated to reduce the levels of laser light reflection after proper alignment of the laser sheet source and the camera so as to prevent damage of the camera and reduce measurements errors. After blade treatment, a number of verification test were carried out (including laser sheet thickness, height of laser sheet with respect to blade position, seeding concentration, laser power, time between pulses and number of images) were carried out to select appropriate test conditions for the main experiments.

Flow seeding was carried out by running the wind tunnel fan and introducing the particles upstream, essentially seeding the entire laboratory housing the wind tunnel. This was found to be the most effective way to achieve adequate seeding concentration and a uniform distribution. The laser was mounted on an elevated and movable platform outside the wind tunnel. The position of the laser sheet plane was approximately midway between the support arm and the blade end. This was selected based on the setting verifications and is within the region that resulted in 2D flow for comparison to CFD results.

2.3 Wind velocity measurements

The measurement of wind speed was carried out using a constant temperature hotwire anemometer (probe model: Dantec Type 55 P16). The hotwire was positioned 0.6m from the bottom wall, 0.5m from the right wall, and 0.4m downstream of the test section inlet. It was calibrated using a Furness Controls FCO510 micro-manometer with an accuracy of 0.25% between 10% (20Pa) and 100% (200Pa) of the reading scale. A Pitot–static probe was connected to the micro-manometer and mounted 0.1m to the left and 0.1m down of the hotwire position. Hotwire measurements were performed across the entire tunnel cross sectional area up to 0.1m from the tunnel walls and the variations in the readings between different positions were within the measurement variation of one position. The reference velocities for the hotwire calibration were derived from the Pitot probe and the

local atmospheric conditions were measured using a digital thermometer and a mercury barometer where measurements were taken at the start of each series of tests. The entire calibration procedure was conducted within 10 minutes of the ambient temperature and pressure measurements to keep the calibration data within similar conditions.

The tunnel fan was run at various constant speeds and at each fan speed, the flow was allowed to settle before any measurements were made. The wind speeds tested covering a range of approximately 3m/s up to 10m/s. For each wind speed, both differential pressure readings from the micro-manometer and voltage readings from the hotwire were recorded for 30s. The highest logging frequency of the micro-manometer was set to 1Hz for all the tests. The hotwire logging frequency was tested at frequencies of 100Hz, 1000Hz, and 10,000Hz. The final logging frequency was set to 100Hz which was determined to be adequate to capture any unsteadiness in the flow velocity. During each test, the first 5 seconds of manometer data was discarded. The average of the last 25s of the manometer data and the 30s of the hotwire data were used in computing the coefficients of King's Law equation (Equation 7) using a simple least-squares curve fitting method as shown in Figure 2c.

$$V^2 = A + B \cdot U^n \quad (7)$$

where V: hotwire voltage
 U: wind speed
 A, B, n: constant coefficients.

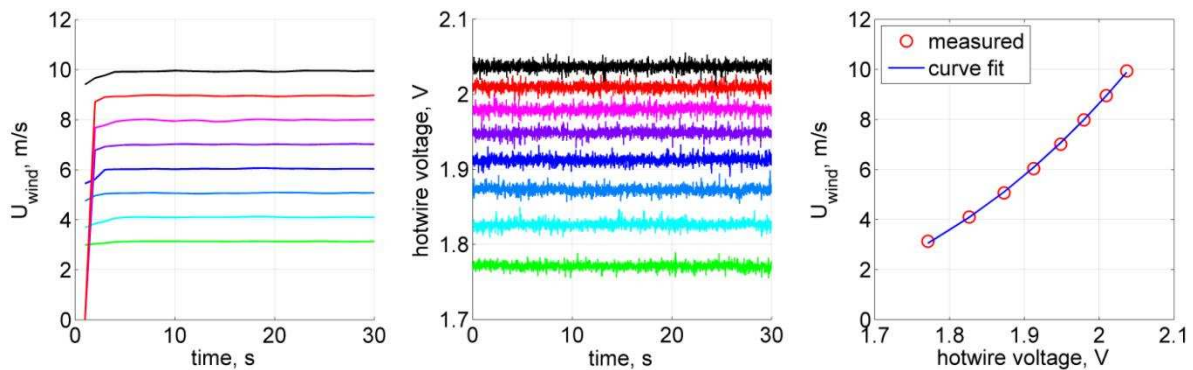


Figure 2. Hotwire velocity traces and calibration using Kings Law.

With a turbulence grid in place at the start of the test section, it was necessary to find the level of turbulence of the flow at the VAWT position since a decay in turbulence intensity will occur between these two points. The hotwire was traversed downstream in increments of 0.2m from its initial position up to near the upstream most position of the VAWT blades at 1.4m from the test section inlet. Figure 3 shows a plot of the measured turbulence intensity at the measurement positions. At the location of the VAWT, the turbulence intensity has dropped to a value of around 1%.

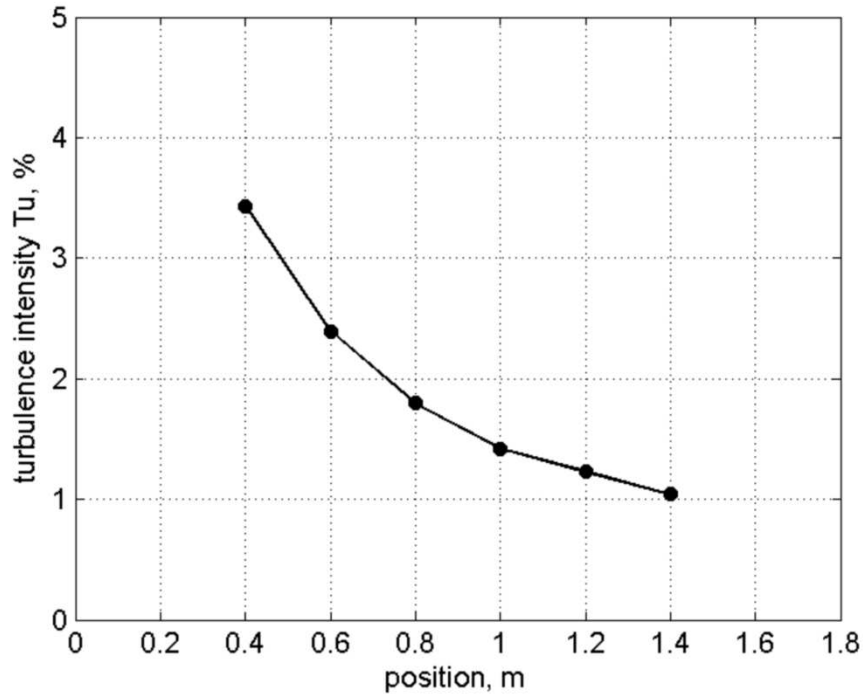


Figure 3. Turbulence intensity in the wind tunnel from the start of the working section.

2.4 Experimental error analysis

The air temperature in the wind tunnel was measured using a digital thermometer. The precision of the thermometer was 0.1°C . The ambient air pressure was also measured using a mercury barometer with a precision of 0.05mmHg . It is necessary to measure both the air temperature and pressure to be able to derive the ambient air density. At standard conditions of 15°C and $101,325\text{Pa}$, an error in temperature of $\pm 0.1^{\circ}\text{C}$ and in pressure of $\pm 0.05\text{mmHg}$ results in a maximum error in air density of about $\pm 0.04\%$. This maximum error is considered to be negligible.

Flow velocity is not measured directly but derived from multiple measurements of the dynamic pressure of the flow in the tunnel and the calibration of a hotwire anemometer which was performed at the start of every test day. Dynamic pressure was read using the micro-manometer which had a precision of 0.01Pa . The flow velocity is derived from the air density and dynamic pressure measurements. The greatest errors in the computation are expected in the lowest velocity region where the accuracy of the pressure readings is just an order of magnitude smaller than the measured values. The maximum error observed is $\pm 0.085\%$. When velocities close to the VAWT operating condition of 7m/s are considered, the maximum error is $\pm 0.017\%$. Similarly, these errors are taken to be negligible.

Errors in flow velocity estimation usually have significant effects on the computed wind power because the relationship is cubic. Despite this, the maximum computed error in wind power is only $\pm 0.06\%$ assuming a rounded-up error of $\pm 0.02\%$ at 7m/s.

When considering flow velocity measurements using the hotwire, a Least Squares fit was utilized to determine the constant coefficients of the King's Power Law relating the hotwire voltage readings to the velocity values derived from the differential pressure readings. Ideally the standard error of both voltage and wind speed should be taken into account. However, the data acquisitions board NI PCI-6220 is a 16-bit DAQ resulting in a negligible precision error. This simplifies the error analysis to inaccuracies in wind speed estimates. With a computed error of less than $\pm 0.5\%$ for wind speed estimates from differential pressure readings, the standard error for the flow velocity estimates using the hotwire was calculated to be $\pm 0.05\text{m/s}$. This resulted in a maximum error in the wind power computations of about $\pm 2.15\%$. Since all measurements required high frequencies of data logging that the micro-manometer is incapable of doing, the hotwire data is taken as the velocity data for all measurements. As such, the errors taken are the hotwire measurement errors.

Accurate measurement of the torque is important when the hysteresis brake is used. From the calibration of the torque sensor, the observed maximum error is $\pm 0.01\text{N}\cdot\text{m}$. The maximum in blade power error due to errors in applied brake readings is $\pm 4.8\%$.

The propagation of all errors in measured and derived variables have a significant effect on the overall estimation of the power coefficient C_p . The major factors that influence the outcome of C_p calculations are the measurements in the applied brake (influencing T_B) and the derived flow velocities U from hotwire voltage readings. These introduce a $\pm 2.15\%$ error in P_w and $\pm 4.8\%$ error in P_B result in a maximum error in C_p value of roughly $\pm 7\%$ (equivalent to $\pm 1\%$ C_p difference).

3.0 Experimental results

3.1 VAWT power coefficient (C_p)

$\sigma = 0.26$ VAWT (Blade 1)

The determined C_p versus λ for the VAWT based on Blade 1 (solidity of 0.26) at three wind speeds is presented in Figure 4 and shows the turbine performance varies considerably with changes in wind speed and λ . The VAWT generates a negative C_p between $\lambda = 1$ and $\lambda = 3.8$ at the tested three wind speeds implying that the VAWT is absorbing rather than generating power in this region. At 6m/s and the lowest Reynolds number, the VAWT generated a negative C_p at all the λ tested, while at 7m/s, positive C_p is attained at $\lambda = 4.3$ and higher. Beyond $\lambda = 3.8$ at 8m/s, the VAWT attained positive C_p and also recorded peak $C_p = 0.15$ at the corresponding $\lambda = 4.75$. These results are entirely in line with earlier investigations at similar conditions.

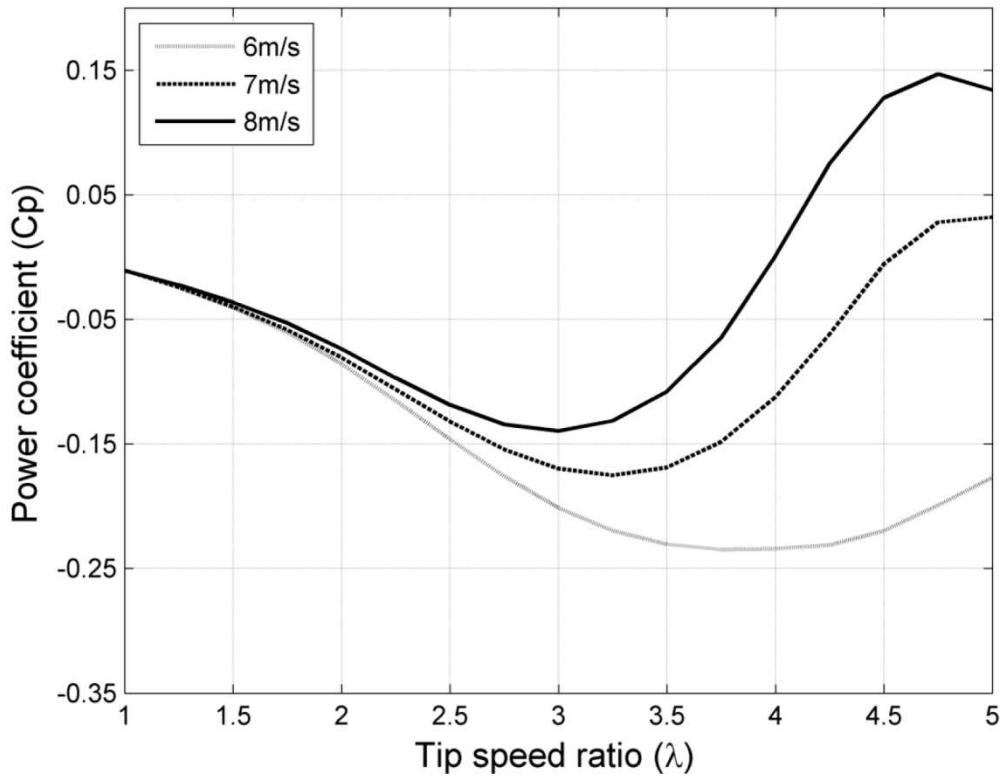


Figure 4. Performance Coefficient (C_p) variation with tip speed ratio for three wind speeds (Reynolds numbers), for turbine based on Blade 1 (solidity = 0.26).

$\sigma = 0.34$ VAWT (Blade 2)

Figure 5 shows C_p versus λ for the Blade 2 based VAWT at the three wind speeds. The VAWT C_p for the three wind speeds is seen to have both negative and positive performance regions as was seen in the previous case (Blade 1). Negative C_p occurs from $\lambda = 1$ to $\lambda = 2.8$ for the 8m/s wind speed case. At the lowest tested 6m/s wind speed, the VAWT attained a maximum $C_p = 0.046$ at $\lambda = 4$ and lowest $C_p = -0.123$ at $\lambda = 2.5$. As the wind speed is increased to 8m/s so is the Reynolds number and the C_p is seen also to increase until the VAWT attained a peak value of $C_p = 0.34$ at $\lambda = 3.75$, higher than the peak C_p attained by the VAWT with Blade 1 (with its lower solidity). At this stage it should be re-iterated that there is a variation in Reynolds number between these tests at the same wind speeds, due to the difference in blade chords.

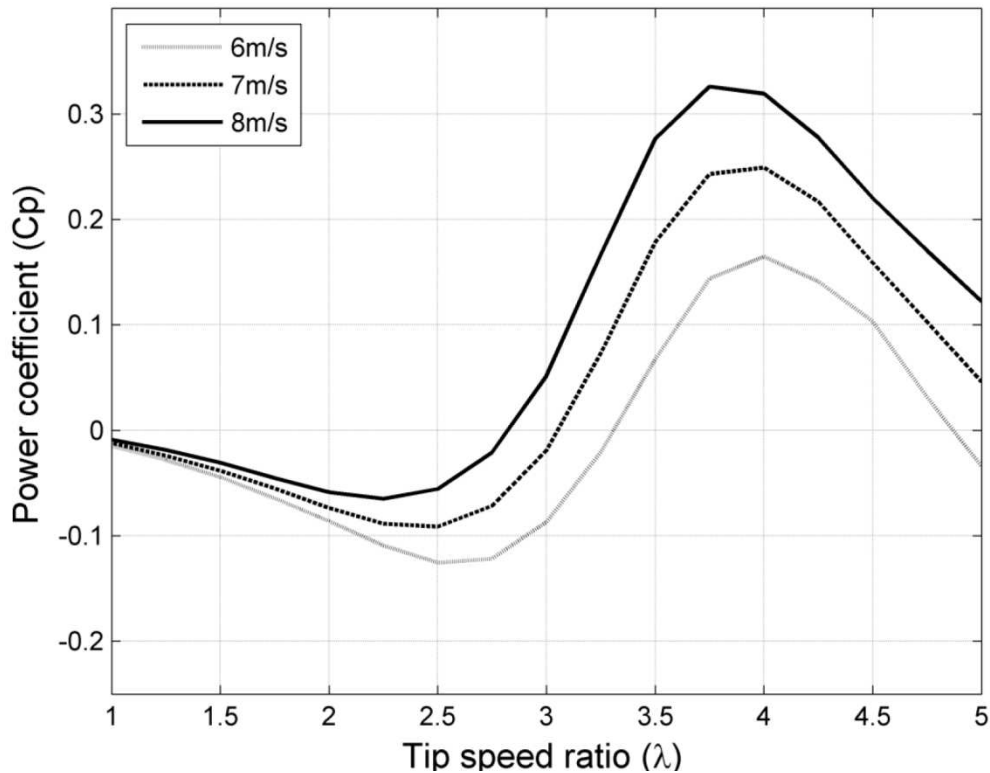


Figure 5. Performance Coefficient (C_p) variation with tip speed ratio for three wind speeds (Reynolds numbers), for turbine based on Blade 2 (solidity = 0.34).

The two performance regions (negative and positive C_p regions) shown for both turbine configurations have previously been seen by Edwards et al. (2012) and Danao et al. (2013) in their studies on a similar VAWT scale. They also show increases in C_p with increase in wind speed and convergence of $C_p - \lambda$ curves at higher wind speeds, indicative of the influence of Reynolds number. The negative C_p region was also seen by Baker (1983), Kirke (1998) and McIntosh (2009). Baker (1983) not only attributed the inability of the VAWT to self-start to the negative performance region, but called the negative C_p region the dead band because power is being absorbed in the region. Also, it can be seen that the performance of the VAWT is dependent on λ , at the lower $\lambda \leq 2.75$ the C_p is clearly in the negative region and peak C_p is attained at the medium λ , while C_p is seen to drop off at the $\lambda \geq 3.95$ irrespective of wind speed and chord length. The effects of solidity on VAWT performance by altering blade chord is discussed in the following section, section 3.3.

3.3. Effects of solidity on performance aerodynamics

Altering any of the three solidity dependent parameter, number of blades, chord length and rotor radius will influence the performance of a VAWT. For this study, the blade chord length was altered and, to eliminate the effects of Reynolds number, the resulting two VAWT configurations were compared at the same Reynolds number to clearly define the effects of solidity alone on VAWT

performance. The Blade 1 based VAWT performance at 8m/s is compared to the performance of Blade 2 based VAWT at 6m/s wind speed (Table 3 and Figure 6), at the same Reynolds numbers at all the tip speed ratios.

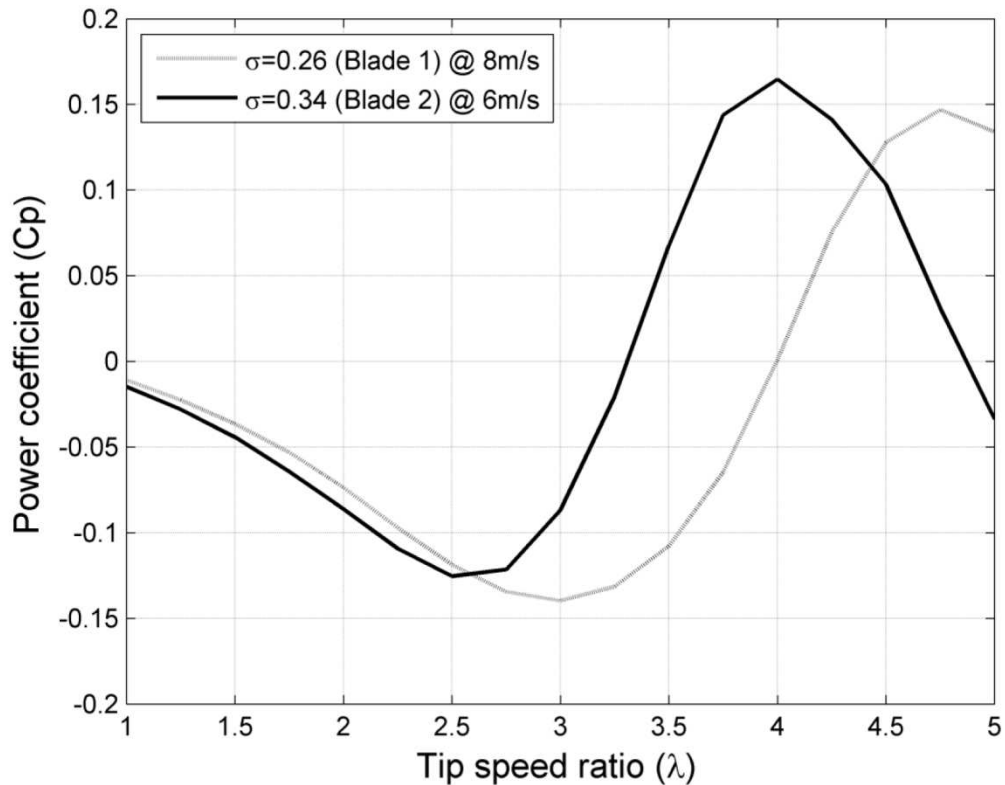


Figure 6. Performance Coefficient (C_p) variation with tip speed ratio for both turbines (solidity = 0.26 and 0.34.) at a wind speed of 8m/s.

Figure 6 compares the C_p of the two VAWTs at various tip speed ratios but at the same Reynolds number. The Blade 1 based VAWT has a wider negative trough that starts from $\lambda = 1$ to $\lambda = 4$, and a positive power region that starts from $\lambda = 4$ and begins to drop off after attaining a peak $C_p = 0.147$ at $\lambda = 4.75$. This VAWT attained a minimum $C_p = -0.14$ at a corresponding $\lambda = 3$. The Blade 2 based VAWT has a narrower negative trough spanning from $\lambda = 1$ to $\lambda = 3.2$ and a positive power region that spanned between $\lambda = 3.2$ and $\lambda = 4.8$, and attained a maximum $C_p = 0.165$ at $\lambda = 4$ and a minimum $C_p = -0.125$ at the corresponding $\lambda = 2.5$.

TSR λ	Blade 1 C_p	Blade 2 C_p	Reynolds Number
1.0	-0.011	-0.019	16,800
1.5	-0.036	-0.047	25,200
2.0	-0.073	-0.088	33,600
2.5	-0.118	-0.125	42,000
3.0	-0.139	-0.87	50,400
3.5	-0.107	0.063	58,800
4.0	0.00	0.165	67,200
4.5	0.127	0.106	75,600
5.0	0.134	-0.377	84,000

Table 3. Compared C_p values and corresponding TSR of the two VAWTs at the same Reynolds number.

The trend of the C_p - λ curves shown in Figure 6 is similar to the results of Templin (1974), and Strickland (1975) in which the momentum models were used for their studies and revealed that; the maximum peak power output remains broadly similar when turbine solidity is reduced and that a lower solidity can widen the C_p - λ operating range of the VAWT. The results also bear close resemblance to the studies of Consul et al, (2009) and McIntosh, (2009) in which numerical models were used. The latter two studies revealed the shift of the entire C_p - λ curve of the higher solidity VAWT to the left, hence attaining maximum C_p at lower λ , while the smaller solidity VAWT attained maximum C_p at higher λ . Although blade chord was altered in this study, similarities are observed in the solidity studies indicating that irrespective of the study method and parameter altered, the effects of solidity on VAWT performance are similar.

None of the previous studies investigated the aerodynamics around the VAWT blades. In this study the blade performance is linked to the aerodynamics of the flow field which helps, for the first time, to provide detailed understanding of why the performance changes between the two turbine solidities.

3.4. Description of C_p and flow fields, $\lambda = 2.5$

PIV measurements of the two VAWT configurations at $\lambda = 2.5$ are shown at a selection of azimuth positions (angles). For brevity, only the most important PIV measurements are discussed, and many others can be found in Eboibi (2013). Figure 7 compares the z – vorticity flow fields of the two VAWTs at the same azimuth positions in the so-called upwind section of rotation. At $\theta = 60^\circ$, blade stall is being initiated by the formation of separation bubble on the inner (lower) side of the Blade 1 ($C = 0.03m$, $\sigma = 0.26$) surface whereas the flow field is seen attached to the Blade 2 ($C = 0.04m$, $\sigma = 0.34$) surface with thinner regions of negative vorticity.

At $\theta = 70^\circ$, the turbine based on Blade 1 experiences deep stall with the leading edge vortex (LEV) seen to have detached from the blade's inner side due to the formation of the trailing edge vortex (TEV) that is already at an advanced stage. At the same conditions for Blade 2 however, the onset of stall is only being initiated with the formation of a small LEV separation bubble. At this azimuth position, the Blade 1 based turbine gains a sudden increase in lift (for a very brief period) that impact positively on the overall performance, while the lift generated by the Blade 2 based turbine is lower but continues to increase steadily until the boundary layer begins to detach from the surface.

Towards the end of the first half of the upwind rotation at $\theta = 80^\circ$, the turbine based on Blade 1 is already shedding pairs of LEV and TEV, and is in the post stall stage dominated by large drag forces. It is apparent that the turbine based on Blade 1 losses lift with the attendant effects of a lowered C_p . Contrary to the flow field around Blade 1 turbine, Blade 2 turbine is stalled with the LEV being pushed away from the blade's surface due to the advanced development of the TEV. At this stage, the Blade 2 based turbine experiences a sudden increase in lift force, though only for a very brief period like that for the Blade 1 based turbine at an azimuth position of $\theta = 70^\circ$, until the start of detachment of the LEV and TEV from the blade's surface which causes an abrupt reduction in lift.

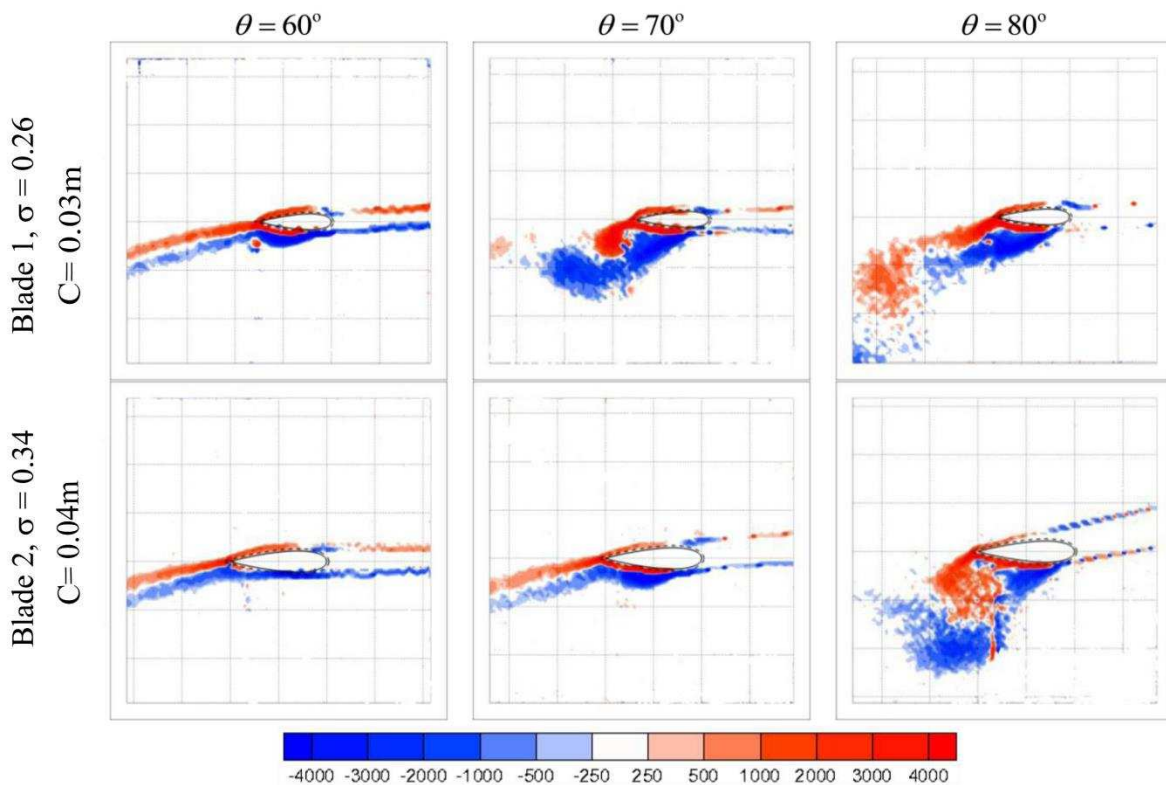


Figure 7. z – vorticity flow fields for the two VAWTs at the same azimuth positions in the upwind section for both turbines at a tip speed ratio of 2.5.

Figure 8 compares z-vorticity for the downwind section of the rotation. It is seen that the flow field for the two turbines configurations bear some similarities as there are no significant differences except for the larger vortex structures of Blade 2. The blades of the two turbines are in a post-stall stage where drag force is dominant. At $\theta = 310^\circ$, reattachment of the LEV on the two blade's surfaces had progressed significantly and the flow fields are seen attached at $\theta = 350^\circ$.

It is shown in Figures 7 and 8 that the flow structures around the blades bears distinct differences at the upwind section and similarities at the downwind section. The flow patterns have strongly influenced the C_p of the two VAWT configurations at $\lambda = 2.5$. Blade 1 stalled at an earlier azimuth angle (before $\theta = 70^\circ$) and also the LEV and TEV are detached completely from the blade's surface in the first half of the upwind section rotation, while Blade 2 stalled later around $\theta = 70^\circ$ with a 10° phase difference, indicating a predominance and shedding of vortices by the smaller blade chord.

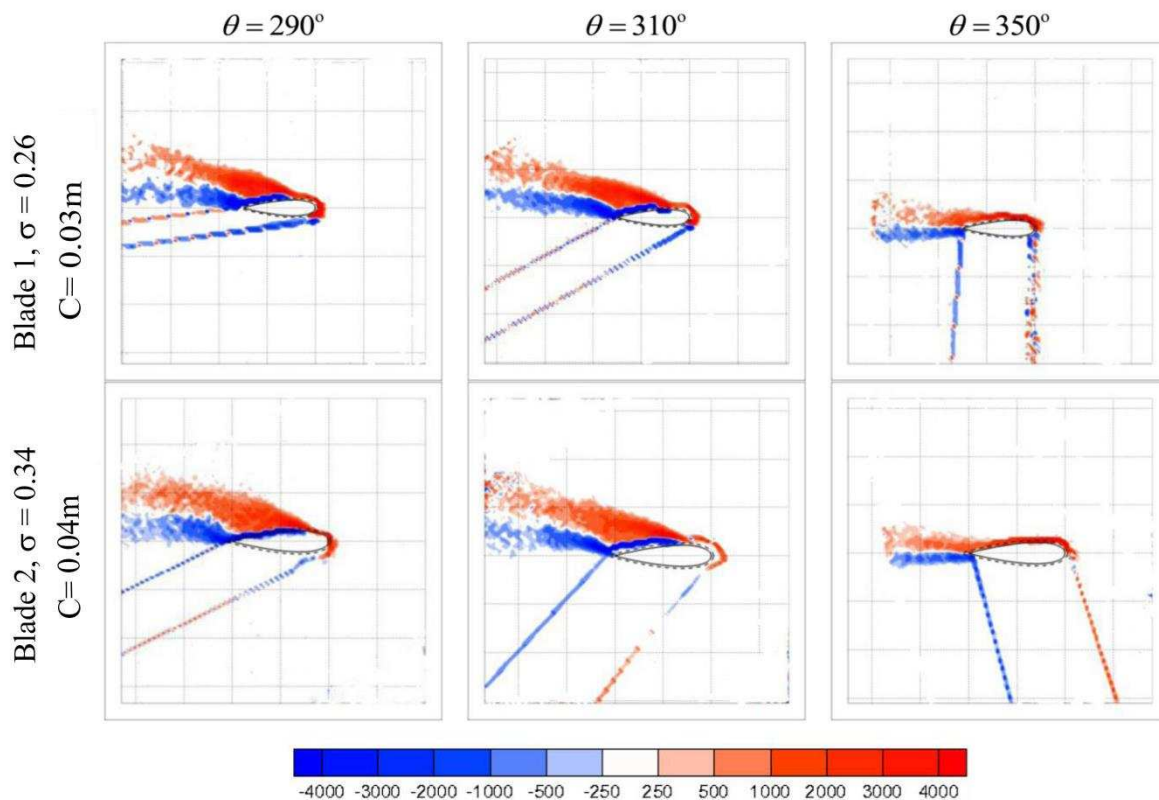


Figure 8. z – vorticity flow fields for the two VAWTs at the same azimuth positions in the downwind section for both turbines at a tip speed ratio of 2.5.

3.5 Description of C_p and flow fields, $\lambda = 3.0$

The C_p of the two VAWT configurations at $\lambda = 3$ is in the negative performance region (Figure 6). The VAWT with the Blade 2 attained a higher $C_p = -0.0869$ while Blade 1 based turbine attained a lower $C_p = -0.14$. The difference in the C_p between the two VAWTs at this λ is around 61% in favour of the higher solidity turbine based on Blade 2. The VAWT C_p at $\lambda = 3$ is linked with the

flow fields aerodynamics to explain the differences observed in the performance between the two VAWT configurations. Figure 9 compares z – vorticity flow fields of the two VAWT blades at the similar azimuth positions in the upwind section of the rotation.

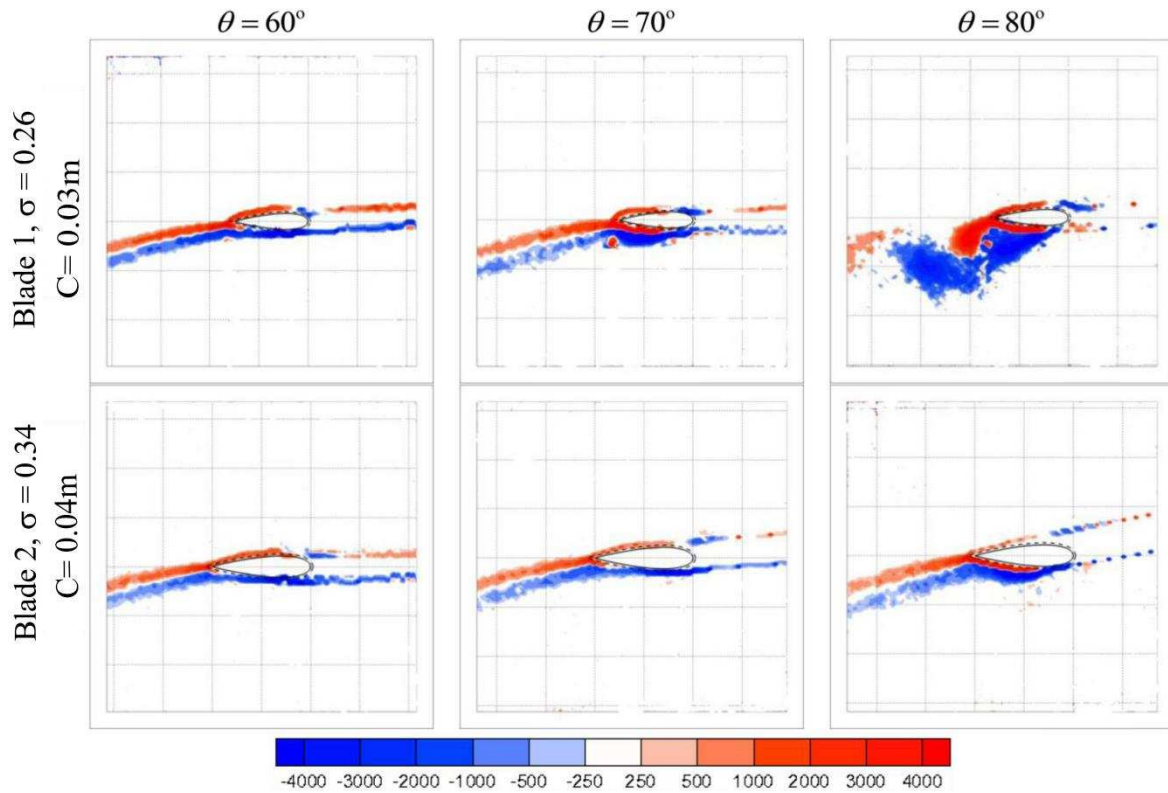


Figure 9. z – vorticity flow fields for the two VAWTs at the same azimuth positions in the upwind section for both turbines at a tip speed ratio of 3.0.

At $\theta = 60^\circ$ the flow around the two blades is fully attached to the surfaces of the two blades. This means that blades of the two VAWT are in the pre-stall stage of the dynamic stall cycle and also that lift force is dominant. The start of dynamic stall is observed by the thickening of the boundary layer resulting in the formation of the separation bubble on the inner side of the Blade 1 based turbine at $\theta = 70^\circ$, whereas the flow field around Blade 2 based turbine is still attached. At $\theta = 80^\circ$, the LEV on Blade 1 based turbine has fully developed and is being pushed away from the blade's surface by the roll up of the TEV whose formation has advanced. Obviously the blade is in deep stall, a situation that causes the lift gained earlier to drop to lower values.

In contrast to the vorticity flow field around Blade 1 ($\sigma = 0.26$) based turbine, the flow around Blade 2 ($\sigma = 0.34$) based turbine is attached, while blade stall is being initiated at $\theta = 80^\circ$. Clearly, the two blades have a phase difference of more than 10 degrees. Further away in the first half of the downwind section of the rotation, the flow features around the two blades bear similar features (Figure 10). The flow fields are characterized by the detachment of the LEV and the TEV from the

blade's surfaces, and also shedding of a pair of vortices, with the onset of flow field reattachment to the blade's surfaces at $\theta = 290^\circ$. The blades are in the post-stall stage of the dynamic stall cycle, and usually at this stage, the drag force is dominant and as a result there is reductions in the lift force and so torque. At $\theta = 310^\circ$, the reattachment of LEV to the surfaces of both blades had advanced considerably, and later on at $\theta = 350^\circ$ the flow fields are seen attached to the surface of the two blades. The performance and flow fields around the blades of the two VAWT configurations at $\lambda = 3$ are quite distinct although some similarities are observed in their flow fields at few blade's azimuth angles.

It can be inferred from Figures 9 and 10 that the C_p of the two VAWT configurations is swayed by the flow physics around the blades. The dynamic stall process for the Blade 1 based turbine started earlier at around $\theta = 70^\circ$ and stalled before $\theta = 80^\circ$ whereas that of Blade 2 based turbine started later, and even at $\theta = 100^\circ$ the LEV was still being pushed away from the blade's surface. This show a phase difference of around 20° higher than the 10° phase difference observed earlier at $\lambda = 2.5$. Consequently, the detachment of the flow fields from the Blade 2 based turbine surface and shedding of pairs of vortices are delayed well into the second half of the upwind section of the rotation with the attendant effects of the higher lift force being sustained longer. This ultimately explains why the higher solidity turbine (Blade 2) performed better than the lower solidity turbine (Blade 1) at $\lambda = 3$.

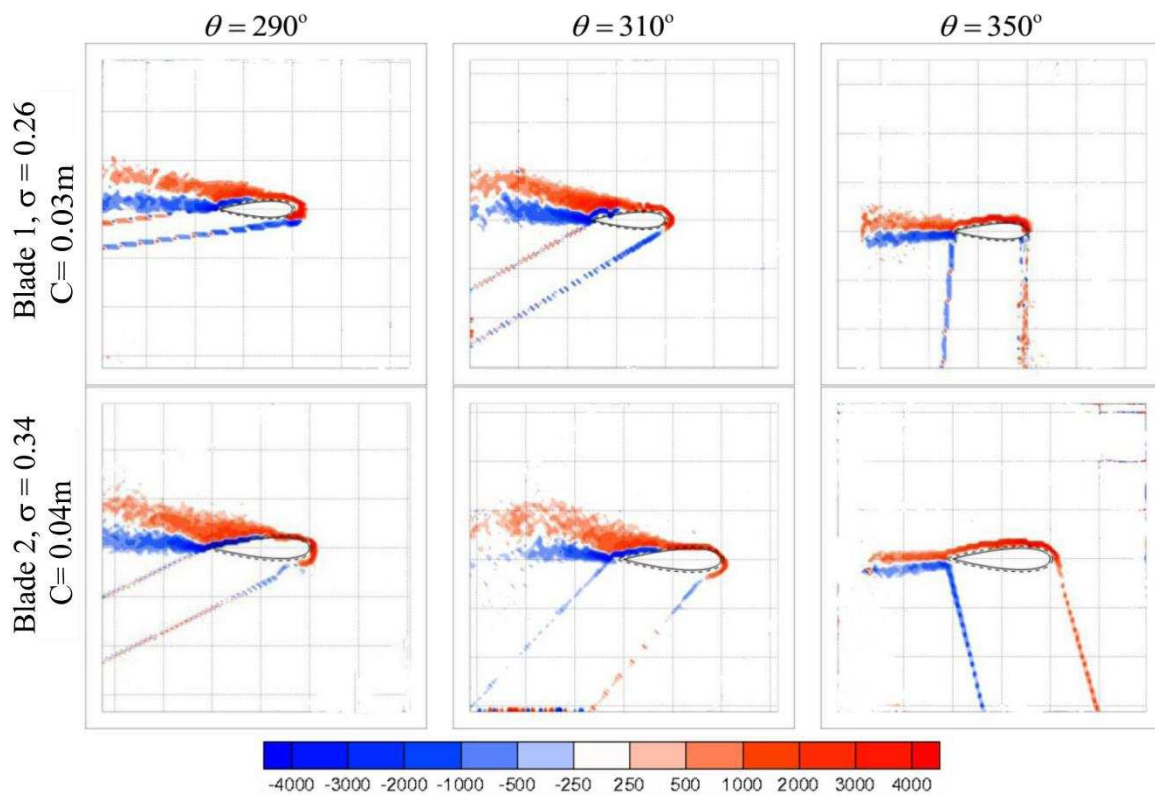


Figure 10. z – vorticity flow fields for the two VAWTs at the same azimuth positions in the downwind section for both turbines at a tip speed ratio of 3.0.

From Figures 7 – 10, the dynamic stall and flow field around the VAWT blades is characterised with the generation of two pairs of stall vortices in one VAWT rotation cycle. The LEV and TEV are generated along the suction and pressure sides of the blades, tip speed ratios and azimuth angles have influenced the development and shedding of stall vortices. All these observations conform to Fujisawa and Shibuya (2001) and Simao Fereira et al. (2009) studies. This study has also revealed that changes in VAWT's solidity due to changes in blade chord can significantly influence stall development, and the entire flow field around a VAWT's blades and ultimately the C_p attained.

4.0 Conclusion

The effects of solidity have been shown by comparing the measured performance and flow field aerodynamics of two VAWTs with different solidities ($\sigma = 0.26$ and 0.34) based on different rotor chord lengths, but at the same Reynolds numbers (ranging from 16,800 to 84,000). The higher solidity turbine has shown steeper and higher gradient C_p - λ curve than that of the lower solidity turbine. In the negative performance region, the $\sigma = 0.26$ VAWT has shown wider C_p - λ curve and lower minimum C_p while the $\sigma = 0.34$ VAWT has a narrower C_p - λ and higher minimum C_p indicating that the self-starting capability of the VAWT can potentially be enhanced by the appropriate selection of VAWT solidity.

The higher solidity VAWT attained better overall C_p than the lower solidity VAWT due to differences in the flow field aerodynamics around the VAWT blades. The blades of the two VAWT configurations have shown significant differences in the thickening of the boundary layer, developments and generation of LEV and TEV, shedding of stall vortices and reattachment of flow to the blades surfaces at $\lambda = 2.5$ and $\lambda = 3$. The earlier start of dynamic stall on the lower solidity VAWT has negative effects on the performance. Selecting appropriate VAWT solidity for a particular wind regime will improve the aerodynamics and energy yield of the VAWT.

Acknowledgements

The authors would like to thank the Mechanical Engineering workshop technicians at the University of Sheffield for their corporation in conducting the experiments. For sponsoring the research, Dr. O. Eboibi would also like to thank the Tertiary Education Trust Funds (TETFund) of Nigeria.

References

Abdul-Malik, I., Garba, I. B., Ngajia, T. B., 2009, Renewable Energy Applications in Nigeria, International Journal of Engineering Science, 1(2), pp. 1-10.

- Baker, J. R., 1983, Features to Aid or Enable Self Starting of Fixed Pitch Low Solidity Vertical Axis Wind Turbines, *Journal of Wind Engineering and Industrial Aerodynamics*, 15(1–3), pp. 369-380.
- Beri, H., and Yao, Y., 2011, Effect of Camber Airfoil on Self Starting of Vertical Axis Wind Turbine, *Journal of Environmental Science and Technology*, 4(3), pp. 302-312.
- Consul, C. A., Willden, R. H. J., Ferrer, E., and McCulloch, M. D., 2009, Influence of Solidity on the Performance of a Cross-Flow Turbine, *Proceedings of the 8th European Wave and Tidal Energy Conference*, Uppsala, Sweden.
- Danao, L. A., 2012, The Influence of Unsteady Wind on the Performance and Aerodynamics of Vertical Axis Wind Turbines, PhD thesis, University of Sheffield, Sheffield, UK.
- Danao, L. A., Eboibi, O., and Howell, R., 2013, An Experimental Investigation into the Influence of Unsteady Wind on the Performance of a Vertical Axis Wind Turbine, *Applied Energy*, 107(0), pp. 403-411.
- Eboibi, O., 2013, The Influence of Blade Chord on the Aerodynamics and Performance Vertical Axis Wind Turbines, PhD Thesis, The University of Sheffield, Sheffield, United Kingdom.
- Eboibi, O., Edwards, J., Howell, R., Danao, L. A., 2014, Development of Velocity Flow Field Measurement Method around a Vertical Axis Wind Turbine Blade Using Particle Image Velocimetry, *Proceedings of the World Congress on Engineering*, London, U.K.
- Edwards, J. M., Danao, L. A., and Howell, R. J., 2012, Novel Experimental Power Curve Determination and Computational Methods for the Performance Analysis of Vertical Axis Wind Turbines, *Journal of Solar Energy Engineering*, 134(3), pp. 11.
- Edwards, J. M., Danao, L. A., and Howell, R. J., 2012 PIV Measurements and CFD Simulation of the Performance and Flow Physics and of a Small-Scale Vertical Axis Wind Turbine, *Wind Energy*, DOI: 10.1002/we.1690.
- El-Samanoudy, M., Ghorab, A. A. E., and Youssef, S. Z., 2010, Effect of Some Design Parameters on the Performance of a Giromill Vertical Axis Wind Turbine, *Ain Shams Engineering Journal*, 1(1), pp. 85-95.
- Fujisawa, N., and Shibuya, S., 2001, Observations of Dynamic Stall on Darrieus Wind Turbine Blades, *Journal of Wind Engineering and Industrial Aerodynamics*, 89(2), pp. 201-214.
- Howell, R., Qin, N., Edwards, J., and Durrani, N., 2010, Wind Tunnel and Numerical Study of a Small Vertical Axis Wind Turbine, *Renewable Energy*, 35(2), pp. 412-422.
- Kirke, B. K., 1998, Evaluation of Self-Starting Vertical Axis Wind Turbines for Stand-Alone Applications, PhD thesis, Griffith University, Gold Coast, Australia.
- Klimas, P. C., 1982, Darrieus Rotor Aerodynamics, *Journal of Solar Energy Engineering*, 104(2), pp 102-105.
- Mays, I., and Holmes, B.A., 1979, Commercial Development of the Variable Geometry Vertical Axis Windmill, *International Power Generation*, Surrey, United Kingdom.
- Mcintosh, S. C., 2009, Wind Energy for the Built Environment, PhD Thesis, Cambridge University, Cambridge, United Kingdom.
- Raciti Castelli M., Betta S.D., and Benini E., 2012, Effect of Blade Number on a Straight-Bladed Vertical-Axis Darrieus Wind Turbine, *World Academy of Science, Engineering and Technology*, 6(1), pp 256-262.

Shedahl, R. E., and Klimas, P. C., 1981, Aerodynamic Characteristics of Seven Symmetrical Airfoil Sections through 180-Degree Angle of Attack for Use in Aerodynamic Analysis of Vertical Axis Wind Turbines. Technical Report No. SAND80-2114, Sandia National Laboratories, Albuquerque, New Mexico.

Simão Ferreira, C. J., Van Kuik, G., Van Brussel, G. J. W., and Scarano, F., 2009, Visualization by PIV of Dynamic Stall on a Vertical Axis Wind Turbine, *Experiments in Fluids*, 46(1), pp. 97-108.

Strickland, J. H., 1975, The Darrieus Turbine: A Performance Prediction Model Using Multiple Stream tubes, Technical Report No. SAND75-0431, Sandia National Laboratories, Albuquerque, New Mexico.

Templin, R. J., 1974, Aerodynamic Performance Theory for the NRC Vertical-Axis Wind Turbine, Technical Report No. LTR-LA-160, National Research Council of Canada, Ottawa, ON, Canada.

List of Figures (All coloured Figures are intended for colour reproduction on the Web and in print.

Figure 1	University of Sheffield wind tunnel facility.
Figure 2	Hotwire calibration plots: a) wind speed calculated from differential pressure readings, b) hotwire voltage readings, c) calibration curve fit.
Figure 3	Turbulence intensity decay in the wind tunnel ($x = 0$: test section inlet).
Figure 4	Power coefficient versus tip speed ratio, $\sigma = 0.26$ VAWT (Blade 1).
Figure 5	Power coefficient versus tip speed ratio, $\sigma = 0.34$ VAWT (Blade 2).
Figure 6	C_p versus λ for the two VAWT configurations at the same Reynolds numbers for each value of λ .
Figure 7	The z-vorticity flow field of PIV measurements of two turbines at $Re = 42,000$ and different azimuth positions for upwind section, $\lambda = 2.5$.
Figure 8	The z-vorticity flow fields of PIV measurements of two chords at $Re = 42,000$ and different azimuth positions in the downwind section, $\lambda = 2.5$.
Figure 9	The z-vorticity flow fields of PIV measurements of two chords at $Re = 50,400$ and different azimuth positions in the upwind section, $\lambda = 3$.
Figure 10	The z-vorticity plots of PIV images of two chords at $Re = 50,400$ and different azimuth positions in the downwind section, $\lambda = 3$.

List of Tables

Table 1	A summary of literature reviewed.
Table 2	Instrumentation used in the turbulence measurement experiments.
Table 3	Compares C_p values and corresponding TSR of the two VAWTs at the same Reynolds number.